Microscopic theory of electron dynamics and time-resolved two-color two-photon photoemission at semiconductor surfaces

A. Zeiser,* N. Bücking, J. Förstner, and A. Knorr
AG Nichtlineare Optik und Quantenelektronik, Institut für Theoretische Physik, Technische Universität Berlin, Hardenbergstrasse 36 PN 7-1, 10623 Berlin, Germany
(Received 3 September 2004; revised manuscript received 8 March 2005; published 10 June 2005)

A microscopic description based on the density matrix formalism is developed to describe the dynamics of photoemission of hot electrons at semiconductor surfaces, including the interaction of bulk and surface states. The equations of motion for the electronic occupations and transitions include the interaction with arbitrary optical fields as well as the electron-phonon coupling. Model wave functions are used to qualitatively describe the bulk-surface dynamics and the subsequent time resolved two-photon photoemission (2PPE) spectra. Our results suggest that it is possible to extract energetic and temporal information of the underlying dynamical occupations of the intermediate states from the 2PPE spectra.

DOI: 10.1103/PhysRevB.71.245309 PACS number(s): 79.60.Bm, 73.20.Mf, 78.47.+p

I. INTRODUCTION

Time resolved two-color two-photon photoemission (TR-2PPE) provides a powerful method for the investigation of dynamic processes in condensed matter, especially at surfaces. In TR-2PPE two pulses of variable temporal delay and different center frequencies (photon energies) interact with the sample. The first pulse excites electrons from occupied into unoccupied states and the second pulse eventually causes emission of these hot electrons into unbound vacuum states. The energy and emission angle of the electrons can be measured and by allowing a variable time delay between the pulses one obtains a time resolved picture of the hot electron distribution.

The TR-2PPE technique has been applied to a variety of situations, ranging from image potential states,[1–5] molecules[6,7] on metal surfaces, bulk states of semiconductors and metals[8–12] to combined dynamics of semiconductor bulk states, surface states,[13–15] and adsorbate states.[16,17] Theoretical descriptions for 2PPE at metals have employed multilevel optical Bloch equations,[1] including phenomenological energy relaxation[18,19] and stationary 2PPE spectra.[20] Dynamical calculations involving photoemission spectra of semiconductors for coherent pulse excitation have been done,[21,22] discussing the influence of final states as well as a phenomenological coupling of bulk and surface states. On the other hand, the microscopic origin of electron transfer due to electron-phonon coupling between bulk and surface has been investigated for incoherent initial conditions.[23]

In this work, a microscopic theory based on the correlation expansion of the dynamical density matrix in second quantization,[24,25] including relevant many particle interactions, will be used to derive equations of motion which determine the surface electron dynamics and the TR-2PPE spectra at semiconductor surfaces. The description includes three-dimensional bulk states, two-dimensional surface states, as well as three-dimensional final (vacuum) states. The many-body interactions are restricted to the electron-phonon interaction (both three-dimensional and two-dimensional phonon modes); however, an extension to include electron-electron interaction is—even if numerically very demanding—straightforward. The coupling to external optical laser fields is treated on a semiclassical basis. Although the second quantization formalism is not necessary for the examination of the optical interaction, thus leading to the same equations as a single particle approach,[26] it is of central importance in the treatment of the phonon-electron interaction, which is necessary to understand recent experiments.[27] Before being specified to a certain material system, the derived equations represent a general description of the electron dynamics at semiconductor surfaces. For the numerical evaluation, typically the restriction to a few-band system is necessary. For this purpose, the single particle states should be calculated from *ab initio* methods.[28] For simplicity and to obtain a first insight in the dynamics of surface electrons, we construct a model system with characteristic model wave functions. A detailed investigation by numerical simulation for different excitation conditions is done to show the interplay of the bulk and surface states after excitation with an electrical field. Finally, to obtain observables, 2PPE spectra are calculated numerically.

Our results suggest that it is possible to extract information of the dynamical populations of the intermediate states (bulk conduction band and surface band) from the 2PPE spectra. Hence, typical time scales of many-body interactions can be derived from a detailed comparison of a series of spectra.

The paper is organized as follows: In Sec. II we introduce our basic surface model for the description of two-dimensional and three-dimensional electronic states. Afterwards, Heisenberg equations for the relevant observables are applied to describe the reduced dynamics of the system using a bath and Markovian approximation for the electron-phonon interaction (Sec. III). Finally, in Sec. IV the model system and wave functions are introduced and numerical results are discussed for various excitation conditions (Sec. V).

II. BASIC SURFACE MODEL

The modeling of the semiconductor surface is done in half space geometry[28–30] interfacing vacuum. Semiconductor and

vacuum are assumed to have the length L, large compared to an elementary cell of the infinite semiconductor. For the description we set up a coordinate system with z perpendicular to the surface, also referred to as the perpendicular part of the position vector $\mathbf{r}$, $r_\perp = z$. The two other directions—x, y—are labeled as the parallel part $\mathbf{r}_\parallel = (x,y)^T$.

By introduction of a surface, the atomic layer at the surface will reorganize, forming a different structure compared to the infinite crystal.[28] However, a translational symmetry in the plane of the surface can be assumed, but none in the perpendicular direction. This is a slightly different approach than that used in *ab initio* state calculations, where a periodical boundary condition at the limits of a slab also induces a translational symmetry perpendicular to the surface. Nevertheless, the symmetry is a subgroup of the translational group of the infinite crystal. Furthermore a reference area S is introduced in the parallel direction. S is large compared to the smallest translational vectors of the surface. The translational symmetry is provided by imposing periodic boundary conditions. Because of this fact, we can use the Bloch theorem in two dimensions to express the wave function as[28]

$$\psi^\alpha_{\mathbf{k}}(\mathbf{r}) = \frac{e^{i\mathbf{k}\cdot\mathbf{r}}}{\sqrt{S}} v^\alpha_{\mathbf{k}}(\mathbf{r}), \tag{1}$$

where v is the Bloch function. $\mathbf{k}$ is a two-dimensional wave vector restricted to the two-dimensional surface Brillouin zone. Furthermore, α labels these two-dimensional bands. In general, α is a multidimensional index.

Surface bands—being two dimensional—can be labeled by a single-component index α. For the bulk bands the description of semiconductors as infinite crystals works well, despite their surfaces. Therefore it is plausible to assume, that the pair $(\lambda, \mathbf{k}^{3d})$, where λ is a three-dimensional band index (e.g., valence band) and $\mathbf{k}^{3d}$ a three-dimensional wave vector can be used for a approximate description of a bulk band. Thus, the wave function of the bulk state will be very similar inside the solid; however, near the surface it will be perturbed and decay outside. In terms of two-dimensional bands, we can express $(\lambda, \mathbf{k}^{3d})$ as $\alpha = (\lambda, k_z^{3d})$ and $\mathbf{k} = (k_x^{3d}, k_y^{3d})^T$. Thereby, we have not accounted for the fact that the surface Brillouin zone will be smaller than the projected bulk Brillouin zone, because of the reconstruction. This means, that there is not a bijective relation between $(k_x^{3d}, k_y^{3d})^T$ and $\mathbf{k}$. However, since in the following we focus on optical excitation close to the Γ resp. $\overline{\Gamma}$ point, we can assume local bijectivity.

Similar arguments can be applied for the description of the phonon modes. Again three-dimensional modes are characterized using a two-dimensional band index κ composed of the original mode and the perpendicular part of the wave vector $\mathbf{q}^{3d}$.

All in all, both three-dimensional-like states as well as two-dimensional states can be expressed in terms of a band index α and a two-dimensional wave vector $\mathbf{k}$. In the next section, we will derive the governing dynamical equations of such a multiband system, including electron-phonon interaction.

III. EQUATIONS OF MOTION

The correlation expansion for the density matrix[24,25,31,32] is applied to describe the dynamics of the system. Using Heisenberg's equations of motion for the expectation values $\langle \hat{A} \rangle = \mathrm{tr}(\rho \hat{A})$

$$-i\hbar \frac{d}{dt} \langle \hat{A} \rangle = \langle [\hat{H}, \hat{A}] \rangle, \tag{2}$$

a set of coupled differential equations for the experimentally observable quantities $\hat{A}$ can be derived. The Hamiltonian $\hat{H}$ includes the free electron and phonon systems, the semiclassical electron-electromagnetic field interaction and electron-phonon contributions

$$\hat{H} = \sum_{\alpha,\mathbf{k}} \hbar \epsilon^\alpha_{\mathbf{k}} a^{\alpha\dagger}_{\mathbf{k}} a^\alpha_{\mathbf{k}} + \sum_{\kappa,\mathbf{q}} \hbar \omega^\kappa_{\mathbf{q}} b^{\kappa\dagger}_{\mathbf{q}} b^\kappa_{\mathbf{q}} - \sum_{\substack{\alpha,\alpha' \\ \mathbf{k},\mathbf{k}'}} \hbar \Omega^{\alpha,\alpha'}_{\mathbf{k},\mathbf{k}'} a^{\alpha\dagger}_{\mathbf{k}} a^{\alpha'}_{\mathbf{k}'} + \sum_{\substack{\alpha,\alpha',\kappa \\ \mathbf{k},\mathbf{k}',\mathbf{q}}} D^{\alpha,\alpha',\kappa}_{\mathbf{k},\mathbf{k}',\mathbf{q}} a^{\alpha\dagger}_{\mathbf{k}} a^{\alpha'}_{\mathbf{k}'} (b^\kappa_{\mathbf{q}} + b^{\kappa\,\dagger}_{-\mathbf{q}}). \tag{3}$$

Here, a and $a^\dagger$ (b and $b^\dagger$) are the creation and annihilation operators of the electrons (phonons), respectively. α is a band index for two-dimensional electronic bands and labels in conjunction with the two-dimensional wave vector $\mathbf{k}$ an electronic state, discussed in Sec. II. Similarly, κ is a two-dimensional phonon mode and $\mathbf{q}$ is a two-dimensional wave vector. The corresponding energies are given by $\hbar\epsilon$ and $\hbar\omega$, respectively. The coupling elements are Ω (Rabi frequency of the electron-light interaction) and D (matrix element of the electron-phonon interaction) and will be specified later (Sec. IV B 2). Expectation values of typical observables are the electronic occupations $\langle a^{\alpha\dagger}_{\mathbf{k}} a^\alpha_{\mathbf{k}} \rangle$ and transitions $\langle a^{\beta\,\dagger}_{\mathbf{k}'} a^\alpha_{\mathbf{k}} \rangle$, $\alpha \neq \beta$ or $\mathbf{k} \neq \mathbf{k}'$. For example, $\langle a^{(f,k_z)\dagger}_{\mathbf{k}} a^{(f,k_z)}_{\mathbf{k}} \rangle$, i.e., the occupation of the vacuum band with wave vector $(\mathbf{k}, k_z)$ is proportional to the photoemission signal. Due to the many body character of the electron-phonon coupling, the equations of motion for the observables are truncated in the correlation expansion[24,25,33] [cf. Appendix A, Eq. (A1)]. Here we only consider correlations up to single phonon assisted density matrices $\langle a^{\alpha'\dagger}_{\mathbf{k}'} a^\alpha_{\mathbf{k}} b^{\kappa(\dagger)}_{\mathbf{q}} \rangle^c$, corresponding to second order Born approximation. Furthermore, we assume that the phonon occupations remain in a thermal equilibrium determined by the temperature T. Thus

$$\langle b^{\kappa(\dagger)}_{\mathbf{q}} \rangle = 0, \quad \langle b^{\kappa\dagger}_{\mathbf{q}} b^{\kappa'\,\dagger}_{\mathbf{q}'} \rangle = 0,$$

$$\langle b^\kappa_{\mathbf{q}} b^{\kappa'}_{\mathbf{q}'} \rangle = 0, \quad \langle b^{\kappa\dagger}_{\mathbf{q}} b^{\kappa'}_{\mathbf{q}'} \rangle = \delta^{\kappa,\kappa'}_{\mathbf{q},\mathbf{q}'} n^\kappa_{\mathbf{q}}(T),$$

where the Bose-Einstein distribution

$$n^\kappa_{\mathbf{q}}(T) = \left[\exp\left(\frac{\hbar \omega^\kappa_{\mathbf{q}}}{k_B T} \right) - 1 \right]^{-1} \tag{4}$$

is used for the expectation values of the phonon occupations, i.e., $n^\kappa_{\mathbf{q}}(T)$.

The electrons are treated in a full nonequilibrium situation. We briefly illustrate the derivation of equations of mo-

tion for the observable quantities directly for the electron transition $\langle a_{\mathbf{k}'}^{\alpha'\dagger} a_{\mathbf{k}}^{\alpha}\rangle$: The equation of motion for the transition couples to the phonon assisted transition $\langle a_{\mathbf{k}}^{\alpha\dagger} a_{\mathbf{k}'}^{\alpha'} b_{\mathbf{q}}^{\kappa(\dagger)}\rangle^c$ [cf. Appendix A, Eq. (A1)]. The Markovian approximation is used to eliminate these quantities from the dynamics. This procedure leads to a closed system of differential equations for the electronic occupations and transitions [cf. Appendix A, Eq. (A2)], which can be separated into two parts

$$\frac{d}{dt}\langle a_{\mathbf{k}}^{\alpha\dagger} a_{\mathbf{l}}^{\beta}\rangle = \left.\frac{d}{dt}\langle a_{\mathbf{k}}^{\alpha\dagger} a_{\mathbf{l}}^{\beta}\rangle\right|_{\text{field}} + \left.\frac{d}{dt}\langle a_{\mathbf{k}}^{\alpha\dagger} a_{\mathbf{l}}^{\beta}\rangle\right|_{\text{coll}}.$$

The first part (field) includes the free motion and the interaction with the electric field ($\Omega_{\mathbf{k},\mathbf{l}}^{\alpha,\beta}$). This contribution reads

$$\left.\frac{d}{dt}\langle a_{\mathbf{k}}^{\alpha\dagger} a_{\mathbf{l}}^{\beta}\rangle\right|_{\text{field}} = i(\epsilon_{\mathbf{k}}^{\alpha} - \epsilon_{\mathbf{l}}^{\beta})\langle a_{\mathbf{k}}^{\alpha\dagger} a_{\mathbf{l}}^{\beta}\rangle - \sum_{\alpha',\mathbf{k}'} \Omega_{\mathbf{k}',\mathbf{k}}^{\alpha',\alpha}\langle a_{\mathbf{k}'}^{\alpha'\dagger} a_{\mathbf{k}}^{\alpha}\rangle + \sum_{\beta',\mathbf{l}'} \Omega_{\mathbf{l},\mathbf{l}'}^{\beta,\beta'}\langle a_{\mathbf{l}}^{\beta\dagger} a_{\mathbf{l}'}^{\beta}\rangle.$$

Here, the Rabi frequency $\Omega_{\mathbf{k}',\mathbf{k}}^{\alpha',\alpha}$ determines the transition strength between different quantum states $(\alpha'\mathbf{k}') \rightarrow (\alpha,\mathbf{k})$.

The second part (coll) contains the electron-phonon interaction and is labeled collision part. As an example, the intuitive contribution of the diagonal scattering terms are discussed here in detail; the general equations are given in Appendix A, Eq. (A2):

$$\left.\frac{d}{dt}\langle a_{\mathbf{k}}^{\alpha\dagger} a_{\mathbf{l}}^{\beta}\rangle\right|_{\text{coll}}^{\text{diag}} = -(\Gamma_{\mathbf{k}}^{\alpha})^{\text{out}}\langle a_{\mathbf{k}}^{\alpha\dagger} a_{\mathbf{l}}^{\beta}\rangle + (\Gamma_{\mathbf{k}}^{\alpha})^{\text{in}}(\delta_{\mathbf{k},\mathbf{l}}^{\alpha,\beta} - \langle a_{\mathbf{k}}^{\alpha\dagger} a_{\mathbf{l}}^{\beta}\rangle) - (\Gamma_{\mathbf{l}}^{\beta})^{\text{out}}\langle a_{\mathbf{k}}^{\alpha\dagger} a_{\mathbf{l}}^{\beta}\rangle + (\Gamma_{\mathbf{l}}^{\beta})^{\text{in}}(\delta_{\mathbf{k},\mathbf{l}}^{\alpha,\beta} - \langle a_{\mathbf{k}}^{\alpha\dagger} a_{\mathbf{l}}^{\beta}\rangle).$$

The scattering rates read

$$(\Gamma_{\mathbf{k}}^{\alpha})^{\text{out}} = \frac{\pi}{\hbar^2}\sum_{\substack{\beta,\kappa,\pm \\ \mathbf{l},\mathbf{q}}} |D_{\mathbf{k},\mathbf{l},\mathbf{q}}^{\alpha,\beta,\kappa}|^2 \delta(\epsilon_{\mathbf{k}}^{\alpha} - \epsilon_{\mathbf{l}}^{\beta} \mp \omega_{\mathbf{q}}^{\kappa}) \times \left(n_{\text{Phon}} + \frac{1}{2} \pm \frac{1}{2}\right)(1 - \langle a_{\mathbf{l}}^{\beta\dagger} a_{\mathbf{l}}^{\beta}\rangle),$$

$$(\Gamma_{\mathbf{k}}^{\alpha})^{\text{in}} = \frac{\pi}{\hbar^2}\sum_{\substack{\beta,\kappa,\pm \\ \mathbf{l},\mathbf{q}}} |D_{\mathbf{k},\mathbf{l},\mathbf{q}}^{\alpha,\beta\kappa}|^2 \delta(\epsilon_{\mathbf{k}}^{\alpha} - \epsilon_{\mathbf{l}}^{\beta} \mp \omega_{\mathbf{q}}^{\kappa}) \times \left(n_{\text{Phon}} + \frac{1}{2} \mp \frac{1}{2}\right)\langle a_{\mathbf{l}}^{\beta\dagger} a_{\mathbf{l}}^{\beta}\rangle.$$

The scattering rates are proportional to $|D|^2$ (second order Born approximation), where D is the electron-phonon interaction matrix element. The delta function results from the Markovian approximation and leads to strict energy conservation in the electron-phonon scattering process. The terms $1-\langle a_{\mathbf{k}}^{\beta\dagger} a_{\mathbf{k}}^{\beta}\rangle$ ensure that the occupations always stay below 1 (Pauli blocking).

Until now, there are no restrictions with respect to the involved electronic states and phonon modes. Hence, specifying these equations (electronic states, phonon modes, and their interaction) to a certain material system and a limited number of relevant states is of use for the description of a photoemission process. Obviously, the best choice to calculate the matrices D and Ω is to use *ab initio* wave functions;[28] however, corresponding calculations are very involved.[34] Therefore, to test our approach within a model situation, the matrix elements have been evaluated for single particle model states. Such an approximation allows a qualitative insight into the coupled dynamics of bulk and surface states as well as their relation to TR-2PPE spectra.

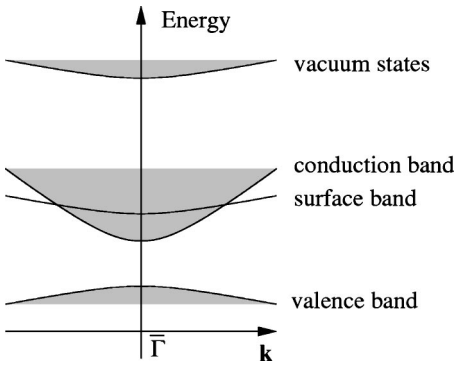

FIG. 1. Sketch of the four band model system.

IV. MODEL SYSTEM

The purpose of the model system is to qualitatively illustrate how the many-body coupling between the bulk and surface states influences the hot electron dynamics as well as the TR-2PPE spectra. For this purpose we introduce a more or less realistic system similar to the reconstructed InP(100) (2×4) mixed dimer surface. There, an unoccupied surface state exists about 0.25 eV above the conduction band minimum with a minimum at the $\bar{\Gamma}$ point.[29,30] There are various reasons that can give rise to the existence of such a surface state. Surface states can be, e.g., explained in rather simple models by the termination of a periodic potential at the surface.[35] Time resolved two-photon photoemission experiments suggest that this surface state couples to the bulk conduction band.[14] Furthermore, the calculated dynamics is restricted to the neighborhood of the $\bar{\Gamma}$ resp. Γ point of the Brillouin zone of direct semiconductors where the energy dispersion can be described within the effective mass approximation. The model system contains four bands as illustrated in Fig. 1.

The electrons initially occupy the three-dimensional valence band. They are excited by the pump pulse into the intermediate and initially unoccupied states consisting of the conduction band (three-dimensional) and the surface band (two-dimensional). The second pulse (probe pulse) partially excites these hot, relaxing electrons to final vacuum states. The occupations in the latter states correspond to the 2PPE signal, which is measured in experiments.[14] As discussed in Sec. II the three three-dimensional bands are labeled as $\alpha = (\lambda, k_z)$, where λ is the usual band index of an infinite semiconductor. Thus we consider the following bands: the three-dimensional bulk bands $\alpha=(\lambda,k_z)$ with $\lambda=v,c,f$ (valence,

conduction, vacuum) and one two-dimensional surface band $\alpha=s$ (surface), all with a two-dimensional wave vector $\mathbf{k}$.

Typically, these bands are coupled via many-body interactions such as electron-electron and electron-phonon scattering. To illustrate the basic dynamics induced in a many-particle surface problem, only the coupling of electrons to LO-phonons is chosen to show the salient features of the coupling as well as their influence on the spectra.

A. Energies and wave functions

We assume that the energy dispersion is isotropic in the directions parallel to the surface and has an extremum at $\bar{\Gamma}$. Thus the energy for all involved states can be written as

$$E_{\mathbf{k}}^{\alpha}=\frac{\hbar^2}{2m_{\mathrm{eff}}^{\alpha}}\mathbf{k}^2+E_0^{\alpha}, \tag{5}$$

where E_0^{α} is the energy offset of the two-dimensional band α and $m_{\mathrm{eff}}^{\alpha}$ is a scalar effective mass. Again, $\alpha=(\lambda,k_z)$ for the bulk states $\lambda=v,c,f$ and $\alpha=s$ for the surface state. For the bulk bands we assume that the original band structure of the infinite semiconductor is retained

$$E_0^{(\lambda,k_z)}=E_0^{\lambda}+\frac{\hbar^2}{2m_{\mathrm{eff}}^{\lambda}}k_z^2,$$

using E_0^{λ} as the original energy offset of the infinite semiconductor and also the original effective mass $m_{\mathrm{eff}}^{\lambda}$. For this case $m_{\mathrm{eff}}^{\alpha}$ in Eq. (5) equals $m_{\mathrm{eff}}^{\lambda}$. For the vacuum electrons the effective mass equals the free electron mass.

The main idea for the construction of the wave functions inside the solid is to take Bloch functions from the infinite crystal with slowly modulated envelope functions, thus conserving many features of the wave functions from the bulk. Outside the solid, the wave functions are either set to zero (surface and bulk bound states) or free electron behavior is assumed (vacuum states). This accounts for the fact that surface-induced effects decay rapidly on the outside of the semiconductor for the bound states. For bulk valence and conduction bands we take the usual Bloch wave functions truncated at the surface. This leads to

$$v^{(\lambda,k_z)}(\mathbf{r})=\begin{cases}\dfrac{e^{ik_z z}}{\sqrt{L}}u^{\lambda}(\mathbf{r}), & z>0\\ 0 & z<0,\end{cases}$$

for $\lambda=c,v$. Similarly, the surface state is also truncated at the surface. Inspired by the density functional theory (DFT) calculations for the InP system under consideration,[29,30] the wave function is modeled to decay exponentially (constant Λ_s) inside the crystal, which leads to

$$v^{s}(\mathbf{r})=\begin{cases}\Lambda_s^{-1/2}e^{-\Lambda_s/2\, z}u^{s}(\mathbf{r}) & z>0\\ 0 & z\leqslant 0.\end{cases}$$

This ansatz is supported by *ab initio* calculations of the wave functions for InP.[36] Here, u^s approximates the real surface wave function and is assumed to be Blochlike. Note, that in first order of the Fröhlich interaction, the orthogonality to the bulk states u^{λ} is not contained (Sec. IV B 2) in this approach. Nevertheless, the use of the model wave functions is a useful assumption if they reproduce the basic system properties, even if they are not strictly orthogonal wave functions. Finally, the free electrons are modeled as incoming waves, which hit the potential barrier of the crystal (finite step potential). In addition, low-energy electron diffraction (LEED) experiments suggest that the free electrons can only penetrate into the crystal to a finite length. Following Mahan,[37] we use incoming LEED states to model the photoemission process. Corresponding wave functions have been calculated.[38] The finite penetration length is reflected by a phenomenological damping (constant Λ_f) of the wave function inside the crystal

$$\bar{v}^{[f,k_z^{(\mathrm{i})}]}(\mathbf{r})=\begin{cases}C_f c_f^{(2)}e^{+ik_z^{(\mathrm{i})}z}u_{f,k_z^{(\mathrm{o})}}(\mathbf{r})e^{-\Lambda_f/2\, z} & z>0\\ C_f\left[e^{+ik_z^{(\mathrm{o})}z}+c_f^{(1)}e^{-ik_z^{(\mathrm{o})}z}\right] & z\leqslant 0,\end{cases}$$

where $k_z\gtrless 0$. The perpendicular part of the inner $[k_z^{(i)}]$ and outer $[k_z^{(o)}]$ wave vector are connected by the energy conservation condition

$$\frac{\hbar^2}{2m_e}[k_z^{(\mathrm{o})}]^2=\frac{\hbar^2}{2m_e}[k_z^{(\mathrm{i})}+G_f]^2+V_0,$$

whereas the parallel part is constant: $\mathbf{k}_{\parallel}^{(\mathrm{o})}=\mathbf{k}_{\parallel}^{(\mathrm{i})}$. Here, V_0 is the height of the finite step potential. Note that, in order to keep $\mathbf{k}^{(\mathrm{i})}$ inside the first Brillouin zone, one must eventually add a reciprocal lattice vector G_f. The other terms read

$$c_f^{(1)}=-[k_z^{(\mathrm{i})}+G_f-k_z^{(\mathrm{o})}]/[k_z^{(\mathrm{i})}+G_f+k_z^{(\mathrm{o})}],$$

$$c_f^{(2)}=2k_z^{(\mathrm{o})}/[k_z^{(\mathrm{i})}+G_f+k_z^{(\mathrm{o})}],$$

$$C_f=(L\{1+[c_f^{(1)}]^2\}+[c_f^{(2)}]^2/\Lambda_f)^{-1/2},$$

$$u_f(\mathbf{r})=e^{iG_f z}.$$

Obviously, the model wave functions are not continuously differentiable (vacuum states) or even not continuous (v, c, s bands). However, they qualitatively reflect the basic features of the real wave functions.[29,30]

B. Interaction matrix elements

With the given set of wave functions from the previous subsection, all matrix elements in the equations of motion, Eqs. (A2) can be calculated. Basically, this is done by splitting the integral into two parts:[31] First, the integral of the slowly varying part (envelopes) and second, the integral over the elementary cell (labeled EC and the corresponding volume V_{EC}). Here we consider the coupling to an external electric field (pump and probe pulse) and the coupling to LO phonons described by the Fröhlich coupling. The detailed calculation for the matrix elements is outlined in the following subsections.

1. Electron-field interaction

Both pump and probe pulse are described as classical electric fields. The interaction with the electronic system is treated via dipole coupling[31]

$$H_{\mathrm{el-E}} = -e\mathbf{r}\cdot\mathbf{E}(t),$$

neglecting the spatial variation of the electric field **E**. This is justified by the fact that the reference length of the solid is smaller than the penetration depth of the light.

Introducing the dipole element

$$\mathbf{d}_{\mathbf{k},\mathbf{k}'}^{\alpha,\alpha'} = \int d^3\mathbf{r}\,\overline{\psi}_{\mathbf{k}}^{\alpha}(\mathbf{r})(e\mathbf{r})\psi_{\mathbf{k}'}^{\alpha'}(\mathbf{r})$$

and the Rabi frequency

$$\Omega_{\mathbf{k},\mathbf{k}'}^{\alpha,\alpha'} = \hbar^{-1}\mathbf{d}_{\mathbf{k},\mathbf{k}'}^{\alpha,\alpha'}\cdot\mathbf{E}(t),$$

the interaction Hamiltonian, Eq. (3), can be written in second quantization as

$$\hat{H}_{\mathrm{el-E}} = -\hbar\sum_{\substack{\alpha,\alpha'\\ \mathbf{k},\mathbf{k}'}}\Omega_{\mathbf{k},\mathbf{k}'}^{\alpha,\alpha'}a_{\mathbf{k}}^{\alpha\dagger}a_{\mathbf{k}'}^{\alpha'}.$$

Using the introduced Bloch functions, Eq. (1), one can simplify the coupling element

$$\mathbf{d}_{\mathbf{k},\mathbf{k}'}^{\alpha,\alpha'} = \delta_{\mathbf{k},\mathbf{k}'}S_{\mathrm{EC}}^{-1}\int \mathrm{d}^3\mathbf{r}\,\overline{v}^{\alpha}(\mathbf{r})(e\mathbf{r})v^{\alpha'}(\mathbf{r}), \tag{6}$$

where S_{EC} is the area of the surface elementary cell. Thus, the electric field only couples states with the same parallel wave vector **k**. The detailed matrix elements are given in Appendix B, Eqs. (B1). As an example, the dipole matrix elements of the conduction band free electron states transition reads

$$\mathbf{d}_{\mathbf{k}^{(c)},\mathbf{k}^{(f)}}^{[c,k_z^{(c)}],[f,k_z^{(f)}]} = \delta_{\mathbf{k}^{(c)},\mathbf{k}^{(f)}}(L_z)^{-1/2}\frac{iC_fT}{k_z^{(f,\mathrm{i})}-k_z^{(c)}+i\Lambda_f/2}\mathbf{d}^{c,f}.$$

As the Kronecker Delta applies only to the parallel parts $\mathbf{k}^{(c)}$ and $\mathbf{k}^{(f)}$, the transition does not conserve the perpendicular part $k_z^{(c)}$ and $k_z^{(f)}$ in general. This is a direct consequence of the surface system and is not valid for bulk materials. Also transitions from states $[(c,k_z),\mathbf{k}]$ to $(s,\mathbf{k})$ for every k_z are possible [cf. the corresponding dipole element in Eq. (B1)]. The remaining terms are defined as

$$\mathbf{d}^{\lambda,\lambda'} = V_{\mathrm{EC}}^{-1}\int d^3\mathbf{r}\,\overline{u}^{\lambda}(\mathbf{r})(-e\mathbf{r})u^{\lambda'}(\mathbf{r}),$$

and are assumed to be known similar to bulk semiconductor optics.[31] In particular, the interband dipole moment between the bulk valence and bulk conduction band can be obtained from literature; all others are chosen to be in the same order of magnitude (cf. Sec. V).

2. Electron-phonon interaction

Here we restrict ourselves to the interaction matrix elements of electrons with longitudinal optical bulk phonons (three-dimensional) and assume a constant energy dispersion relation $\hbar\omega_{\mathbf{q}^{3d}}^{\mathrm{LO}}=\hbar\omega^{\mathrm{LO}}$.

Similar to the bulk electrons, the phonon field is expanded into modes which are represented by traveling waves. We assume for simplicity that the modes are not disturbed by the surface. In this approximation, the Fröhlich coupling leads to

$$D_{\mathbf{k},\mathbf{k}',\mathbf{q}^{3d}}^{\alpha,\alpha',\mathrm{LO}} = \sqrt{\frac{e^2\hbar\omega_{\mathrm{LO}}}{2SL\varepsilon_0\epsilon_{\mathrm{Phon}}}}\int \mathrm{d}^3\mathbf{r}\,\overline{\psi}_{\mathbf{k}}^{\alpha}(\mathbf{r})\frac{e^{i\mathbf{q}\cdot\mathbf{r}}}{|\mathbf{q}^{3d}|}\psi_{\mathbf{k}'}^{\alpha'}(\mathbf{r}).$$

Here, $\epsilon_{\mathrm{phon}}=(\epsilon_\infty^{-1}-\epsilon_0^{-1})^{-1}$, with ϵ_0 (ϵ_∞) being the lower (higher) frequency limit of the dielectric function and ε_0 the vacuum dielectric constant. Again using the Bloch functions Eq. (1), one obtains

$$D_{\mathbf{k},\mathbf{k}',\mathbf{q}^{3\mathrm{d}}}^{\alpha,\alpha',\mathrm{LO}} = \sqrt{\frac{e^2\hbar\omega_{\mathrm{LO}}}{2SL\varepsilon_0\epsilon_{\mathrm{Phon}}}}\delta(\mathbf{k}'-\mathbf{k}+\mathbf{q}_{\parallel}^{3\mathrm{d}}) \times \underbrace{S_{\mathrm{EC}}^{-1}\int \mathrm{d}^3\mathbf{r}\,\overline{v}^{\alpha}\frac{e^{iq_zz}}{|\mathbf{q}^{3\mathrm{d}}|}v^{\alpha'}}_{\Delta_{q_z^{3\mathrm{d}}}^{\alpha,\alpha'}}.$$

The remaining integral $\Delta_{q_z^{3\mathrm{d}}}^{\alpha,\alpha'}$ can be evaluated using the explicit wave functions of Sec. IV A and is given in Eq. (B2). The remaining constant

$$D^{c,s} = V_{\mathrm{EC}}^{-1}\int d^3\mathbf{r}\,\overline{u}^{c}(\mathbf{r})u^{s}(\mathbf{r}) \tag{7}$$

affects the coupling strength of the phononic bulk-surface band coupling. If orthogonality between the Bloch function of the bulk conduction band and the surface band is assumed, the two bands would not couple. Since it is normalized, the Cauchy-Schwartz inequality restricts the coupling to $|D^{c,s}|\leqslant 1$. In Sec. V, this value will be varied to discuss the influence of the coupling strength. A more sophisticated approach will obtain these values from *ab initio* calculations.

C. Equations of motion for the model system

Using the calculated matrix elements [Eqs. (B1) and (B2)] the equation of motion, Eqs. (A2), can be further simplified for the considered four-band system. First of all, due to Eq. (6), only transitions $\langle a_{\mathbf{k}'}^{\alpha'\dagger}a_{\mathbf{k}}^{\alpha}\rangle$ with the same parallel wave vector $\mathbf{k}'=\mathbf{k}$ are excited. However, interband polarizations with different k_z (included in the index α) have to be taken into account. For spatially homogeneous excitation of bulk material, such terms are typically zero. Thus, a type of quantum coherence occurs in the description of a surface. Second, the process induced by the pump and the probe pulses can be separated: The photon energy of the pump pulse is of the order of the band gap energy, exciting electrons from the bulk valence band into the surface and bulk conduction band, leaving the vacuum states almost unpopulated because of the large detuning. Similar arguments apply to the second pulse (probe pulse), which is energetically close to the transition energy between surface/conduction bulk band and vacuum states. Hence, it does not excite electrons from the bulk valence band. Therefore, for the numerical evaluation, both excitation processes can be calculated in separated subsystems. The first subsystem (pump pulse) includes valence, conduction bulk, and surface band, while the second system (probe pulse) is composed of conduction bulk and conduction sur-

face band, as well as free electron states. Third, the probe pulse is assumed to be weak enough to not affect the populations of the bulk and the surface band. Finally, the equations of motion are treated in the rotating wave approximation (RWA),[39] considerably reducing the computational effort. For the second system (conduction bulk and surface band, vacuum electrons) the equations of motion caused by the free motion and the electric field are given in Appendix C. The treatment of the other subsystem is analogous.

The only difference between the investigated subsystems is that the electron-phonon interaction occurs within and in between the bulk valence and conduction bands, and the surface band (the phonon interaction can be restricted to the first subsystem). One example of the corresponding diagonal equations of the collision part (bulk-surface scattering) is given in Appendix D, Eq. (D1). There, the constant dispersion of the LO phonons and the isotropy can be used to simplify the equations.

All in all, the pump pulse is calculated in the first subsystem containing bulk valence and conduction, and surface band including the electron-phonon scattering. The occupations of the bulk conduction band, as well as for the surface band, which vary in time, are used as input parameters for the calculation of the response to the second pulse. This has proved to be very advantageous for the numerical computation, since the RWA can be applied to each subsystem.

V. NUMERICAL SIMULATION

In this section the derived equations of motion for the four band system, cf. Appendix C and Appendix D, will be solved numerically for different excitation conditions, applying a fourth order Runge-Kutta algorithm with a time step of 1 fs. The wave number k space (k_z and $|\mathbf{k}_\parallel|$) has been discretized by 201×101 points for the area $[-1\ \mathrm{nm}^{-1}, 1\ \mathrm{nm}^{-1}]\times[0\ \mathrm{nm}^{-1}, 1\ \mathrm{nm}^{-1}]$. This discretization leads to a length of the crystal of approximately 600 nm. Note that Δk_z should be chosen, according to the total length L corresponding to the penetration length of the pump pulse. Furthermore, only diagonal scattering terms (cf. Sec. III) have been taken into account. The set of used parameters is given in Table I.

In the following, two different excitation situations are investigated: (i) resonant excitation into the surface band ($E_{\mathrm{pump}}=1.614$ eV), (ii) excitation into the conduction band, energetically well above the surface band ($E_{\mathrm{pump}}=1.839$ eV). In both cases, the dynamics of the carrier distribution is investigated as well as the resulting 2PPE spectra at several delay times between the pump and the probe pulse. For both investigated situations the pump pulse has 40 fs full width at half maximum (FWHM) and is centered at 0 fs while the probe pulse has its mean energy at $E_{\mathrm{probe}}=6.461$ eV and has a width of 60 fs (FWHM).

To understand the subsequently calculated 2PPE-spectra, first the carrier dynamics induced by the pump pulse is investigated (Sec. V A). Here, the focus is on the coupling and the electron transfer dynamics between the conduction bulk and surface band. Afterwards, Sec. V B is focused on the TR-2PPE spectra of the emitted electrons (induced by the probe pulse). The simultaneous consideration of the temporal dynamics of the spectra and the carriers allows us to clarify to what extent electron transfer rates can be extracted from experimental observables.

TABLE I. Parameters used.

	Unit	Value
E_0^v	eV	0[a]
E_0^c	eV	1.339[a]
E_0^s	eV	1.589[b]
E_0^f	eV	7.7[c]
m_{eff}^v	m_e	−0.45[a]
m_{eff}^c	m_e	0.078[a]
m_{eff}^s	m_e	0.2
m_{eff}^f	m_e	1
Λ_s	nm^{-1}	0.5[b]
Λ_f	nm^{-1}	2.4[d]
ϵ_0	1	9.52[a]
ϵ_∞	1	12.35[a]
T	K	300
$\hbar\omega_{\mathrm{LO}}$	meV	43[a]
$d^{v,c}$	e nm	0.3[e]
$d^{v,s}$	e nm	1.2/0.0[e]
$d^{c,f}$	e nm	0.3[f]
$d^{s,f}$	e nm	0.09[f]

[a]See Ref. 40.
[b]See Ref. 30.
[c]See Ref. 41.
[d]See Ref. 42.
[e]To reproduce experimental results (Ref. 14), the dipole moment of the transition valence-surface band is set four times the dipole moment valence-conduction band for situation (i). This ensures that mainly the surface state is occupied and not the isoenergetic bulk states. However, for situation (ii), the dipole moment is set zero to ensure a clean initial condition.
[f]These parameters affect the strength of the signal in the 2PPE spectra, and are chosen so that both signals (surface and bulk) are balanced.

A. Photoinduced surface-bulk dynamics

To obtain a first insight into the dynamics, Fig. 2 shows the total number of electrons in the surface band $n_{\mathrm{total}}^s=\Sigma_{\mathbf{k}}\langle a_{\mathbf{k}}^{s\dagger}a_{\mathbf{k}}^s\rangle$ as a function of time for both model situations (i) and (ii). Due to the different time scales for both cases, it can be recognized, that the initial growth of the electron number in the surface band is caused by the pump pulse (i) or electron-phonon scattering from bulk into surface states (ii). The subsequent decay of both signals is determined by the electron scattering from surface into bulk states.

For discussion of the detailed dynamics, we focus first on situation (i). Here the pump pulse populates the surface states directly and the maximum population is reached at approximately the same time as the peak of the pump pulse (dashed vertical line in Fig. 2). Subsequently, the electrons scatter from the surface into the bulk conduction band and

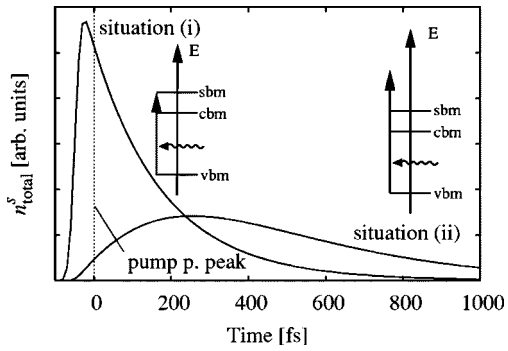

FIG. 2. Total number of electrons in the surface band for resonant excitation into the surface band [situation (i)] and bulk excitation [situation (ii)].

vacate the surface band, causing the exponential decay of the electron occupation on a 200 fs time scale. In Fig. 3, the carrier occupations of the surface states and the bulk conduction band are plotted as a function of energy (for the bulk conduction band we take $E=E^{c,k_z}_{\mathbf{k}}|_{k_z=0}$, see below for the discussion of the usefulness of this quantity) and time. It can be recognized that initially populated surface states (peak at 0.25 eV above the conduction band minimum) are depopulated due to an energetically favored effective scattering from the surface band into the bulk conduction band (evolving peak at zero energy). In the course of time (several hundred femtoseconds), all carriers equilibrate into a Fermi Dirac distribution at the bottom of the conduction band. The distributions shown in Fig. 3 are plotted for $k_z=0$, i.e., only the in-plane component is depicted. Although in general, quantities that involve three-dimensional bands depend not only on the magnitude of the wave vector $\mathbf{k}^{3d}$ but in general also on the angle between (k_x^{3d},k_y^{3d}) and k_z^{3d}, the discussion of the occupation at $k_z=0$ is a useful approach since it can be shown numerically that those anisotropy effects are of minor importance. In Fig. 3, however, the occupations for the bulk conduction band are taken for $k_z=0$; this reduction of information assumes that the discussed anisotropy is not of major importance. To investigate the strength of this anisotropy, the occupations for the bulk conduction band are given at a fixed time in Fig. 4, for the extreme situations $k_\parallel=0$ or $k_z=0$, respectively, hardly showing anisotropy. The small anisotropy can be explained by the fact that typically more electrons occupy the bulk conduction band compared to the occupation of the surface band (cf. Fig. 5).

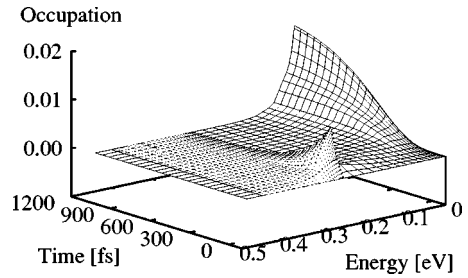

FIG. 3. Occupation of bulk states ($k_z=0$, minimum at 0 eV) and surface states (minimum at 0.25 eV) for resonant surface band excitation [situation (i)].

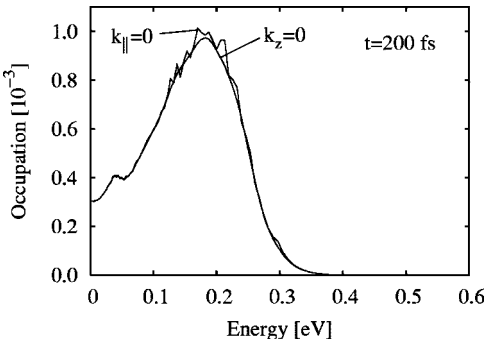

FIG. 4. Anisotropy for excitation into the conduction band at $t=200$ fs. Occupations for $k_z=0$ and $\mathbf{k}_\parallel=0$.

A detailed numerical analysis shows that the dominance of the three-dimensional bulk conduction band prevents a distinct formation of anisotropy.

After the discussion of the direct surface state excitation (i), second, the dominant excitation of the bulk conduction band states is analyzed [situation (ii)]. Because of the richer dynamics, we focus on excitation of continuum states well above the position of the surface state. Additionally, to have a clean initial situation, i.e., to prevent direct excitation of valence electrons into the surface state, the corresponding dipole element has been set to zero. In Fig. 6 it can be seen that at the beginning of the dynamics, the carriers are injected into high energy states in the conduction band (peak at $t=0$ and $E=0.4$ eV). The subsequent dynamics (Fig. 6) can be characterized as follows: The optically excited bulk electrons relax within several tens of femtoseconds in the bulk conduction band and undergo a transfer process from energetically higher states into states which are isoenergetic (or within the phonon energy) with the surface band. Therefore, the surface band can be populated ($E=0.25$ eV, $t=100$ fs). At the same time also electron-phonon scattering in the surface band takes place, leading to electron equilibration inside the surface band. Later on, the carriers undergo a transfer from the surface state to the conduction band minimum (third peak evolving after about 400 fs at 0 eV). As a consequence of these back and forth scattering processes between the bands, the electrons are temporarily trapped at the surface and a delay occurs in the total equilibration and cooling pro-

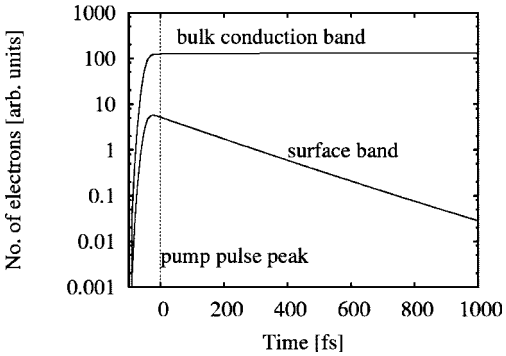

FIG. 5. Logarithmic plot of total number of electrons in the surface and bulk conduction band for resonant excitation into the surface band [situation (i)].

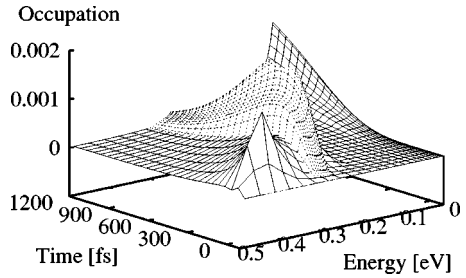

FIG. 6. Occupation of bulk states ($k_z=0$, minimum at 0 eV) and surface states (minimum at 0.25 eV) for conduction band excitation [situation (ii)]. To illustrate the dynamics more clearly, the bulk contribution for the band minimum ($E \leqslant 0.2$ eV) has been multiplied by a factor 0.1.

cess of the initially excited bulk states. Again, investigation of the surface induced spatial anisotropy shows nearly no difference for different directions (not shown). Similar to situation (i), this can again be explained by the small number of states in the surface band compared to the conduction band.

B. TR-2PPE spectra

After the discussion of the carrier dynamics for the two different excitation situations (i) and (ii), the question arises whether the observed occupation dynamics is also reflected in the experimentally observable 2PPE spectra. This would allow one to draw conclusions from the experimental spectra concerning the energetics and the time scales of microscopic scattering and electron transfer mechanisms. For example, the electron transfer dynamics between different bands is determined by the coupling strength between the involved bands.

To investigate the effect of different coupling strengths in the TR-2PPE spectra, the coupling constant between the surface and the conduction band $|D^{c,s}|^2$, cf. Eq. (7), is varied for all calculated spectra from 0.1 up to 4.0. The strong coupling limit is treated to examine a even stronger coupling than the LO phonons allow on their own (Cauchy-Schwartz inequality), thus modeling the influence of more involved phonon modes. For the spectra we have chosen electron emission perpendicular to the surface ($\mathbf{k}_\parallel=0$). The probe pulse has its mean energy at $E_{\text{probe}}=6.461$ eV and has a width of 60 fs (FWHM).

Again, we start with the analysis of situation (i), i.e., the direct surface state excitation via the pump pulse. In Fig. 7 the resulting 2PPE spectra for the resonant excitation of the surface band are displayed for various delay times and coupling strengths (compare figure caption).

The two peaks at 0.1 and 0.35 eV arise from the minimum of the bulk conduction band and surface band, respectively. The conduction band minimum appears at 0.1 eV since the energy of the probe pulse, E_{probe}, is chosen 100 meV larger than the difference between E_0^c (conduction band minimum) and V_0 (height of the step potential). Since only perpendicular emission is treated $\mathbf{k}=0$, only the electron emission from the surface band minimum (at $\mathbf{k}=0$) can be observed in the spectra. 0.25 eV above the bulk conduction band minimum

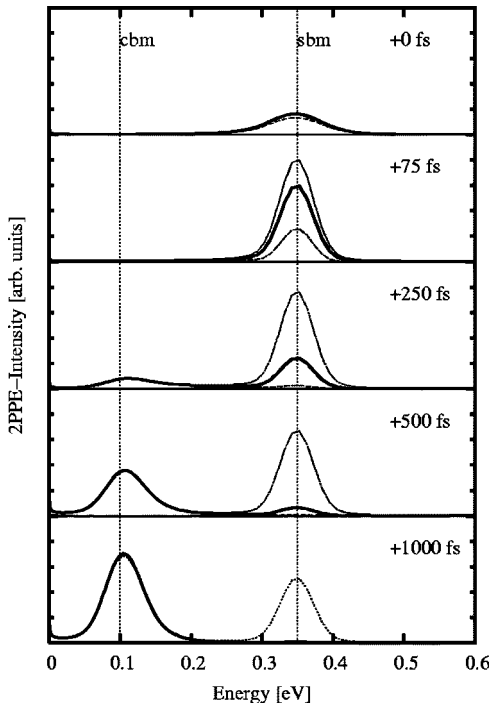

FIG. 7. Photoemission spectra for coupling strength $|D^{c,s}|^2=1.0$ (solid thick line), $|D^{c,s}|^2=0.1$ (dotted line), and $|D^{c,s}|^2=4.0$ (dashed line) and various time delays (see insets) for resonant excitation into the surface state [situation (i)]. The minimum of the surface (bulk conduction) band is located at 0.35 eV (0.1 eV).

corresponding to the used probe pulse, the evaluated surface band minimum appears at 0.35 eV in the photoemission spectra. Strict energy conservation in the electron-photon interaction would lead to an abrupt truncation below 0.1 eV and a Dirac delta-like peak at 0.35 eV, but because of the finite duration of the probe pulse, the peaks are broadened mainly by the spectral width of the probe pulse. In the following, we first focus on the thick line in Fig. 7, corresponding to the standard (Sec. V A) coupling strength of $|D^{c,s}|^2=1.0$. At the beginning, as the peaks of both pulses coincide ($t=0$ fs), almost all electrons populate the surface band or isoenergetic bulk conduction band states. Hence, only a signal at 0.35 eV occurs. The surface state related peak develops its maximum at a time delay of $t=75$ fs, occurring from the time convolution of the 40 fs pump and the 60 fs probe pulse. Later on, the signal decay at 0.35 eV can be related to the electron relaxation into the bulk conduction band. A signal at 0.2–0.3 eV indicates the occupation of the corresponding bulk conduction band states reaching appreciable values from 250 to 500 fs. In the final spectra (1000 fs), the equilibrium situation (all electrons in a Fermi-Dirac distribution in the bulk conduction band) has been reached.

The time dependence of the signal peak that results from the surface band emission (0.35 eV) is separately displayed in Fig. 8 (logarithmic scale).

It can be recognized that this signal is clearly affected by the coupling strength between bulk and surface band. Therefore we may conclude, that the temporal decay of the surface signal allows the extraction of typical coupling strength from the time dependence of the 2PPE signals. To illustrate this in

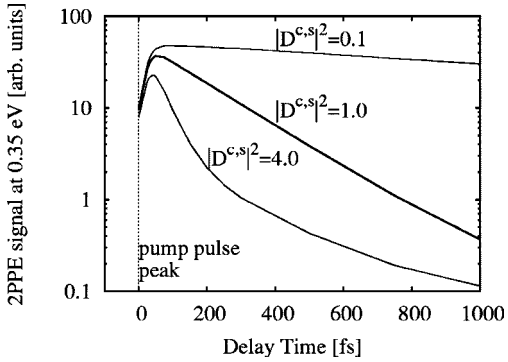

FIG. 8. 2PPE-signal at 0.35eV (originated from surface band) for resonant excitation into the surface state [situation (i)] over delay time for different coupling strengths: $|D^{c,s}|^2=0.1$, $|D^{c,s}|^2=1.0$, and $|D^{c,s}|^2=4.0$.

more detail, the depopulation of the total numbers of surface electrons, n^s_{total} (cf. Sec. V A), as well as the TR-2PPE signal at 0.35 eV are fitted with an exponential function. The obtained decay rates are shown in Table II.

Both constants are in good agreement, and the decay rate Γ is approximately given by

$$\Gamma \approx 5.5 \times 10^{-3}|D^{c,s}|^2 \text{ fs}^{-1}.$$

Such a result may even validate future rate equation treatments of the 2PPE signal. The simple picture of an exponential decay proportional to $|D^{c,s}|^2$ holds, as long as the scattering out of the surface dominates the depopulation: For the strong coupling $|D^{c,s}|^2=4.0$, the decay slows down after about 170 fs. Here, surface band and bulk conduction band states are in a dynamical quasiequilibrium, reducing the scattering rates: The faster coupling between the surface band and the bulk conduction band allows the occupation of the surface band to follow only adiabatically the slower relaxation inside the bulk conduction band. Hence, the intraband relaxation within the bulk conduction band determines the depopulation of the surface band.

In contrast to the signal from the surface band, the signal which arises from the minimum of the bulk conduction band (cf. Fig. 7, at about 0.1 eV) is hardly affected by the coupling constant between surface and bulk states, because the small number of electrons in the surface state barely effect the electron relaxation in the bulk conduction band.

After the discussion of the direct excitation of the surface state, we focus on the excitation of bulk states energetically well above the surface states using a pump pulse with energy

TABLE II. Exponential decay constants [$\exp(-\Gamma t)$] of the total numbers of electrons $n^s_{\text{total}}(\Gamma_{n^s_{\text{total}}})$ and of the TR-2PPE signal at 0.35 eV (Γ_{signal}).

$\lvert D^{c,s}\rvert^2$	$\Gamma_{n^s_{\text{total}}}$ (fs^{-1})	Γ_{signal} (fs^{-1})
0.1	$5.39\cdot10^{-4}$	$5.59\cdot10^{-4}$
1.0	$5.48\cdot10^{-3}$	$5.28\cdot10^{-3}$
4.0	$1.86\cdot10^{-2}$	$1.55\cdot10^{-2}$

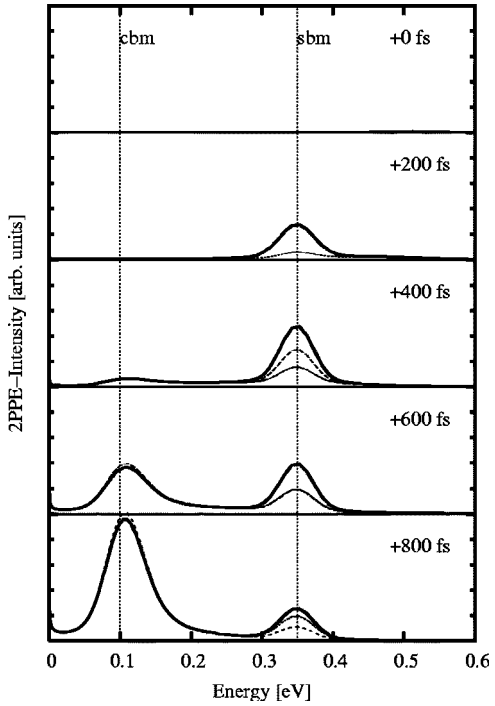

FIG. 9. Photoemission spectra for coupling strength $|D^{c,s}|^2=1.0$ (solid thick line), $|D^{c,s}|^2=0.1$ (dashed line), and $|D^{c,s}|^2=4.0$ (dotted line) and various time delays (see insets) for excitation into bulk conduction band [situation (ii)]. The minimum of the surface (bulk conduction) band is located at 0.35 eV (0.1 eV).

$E_{\text{pump}}=1.839$ eV [situation (ii)]. Figure 9 shows the corresponding TR-2PPE spectra. The corresponding logarithmic plot of the peak of the surface signal peak at 0.35 eV is displayed in Fig. 10.

Again, the TR-2PPE signal at the conduction band minimum does not differ for the various coupling strengths, as the dynamics of the electrons in the bulk conduction band is hardly affected by the interaction with the surface states. Furthermore, the dynamics of the bulk conduction band electrons having larger energies than the surface states can hardly be seen in the spectra (only a weak energy shoulder above the surface band minimum is observed). Note, however, that

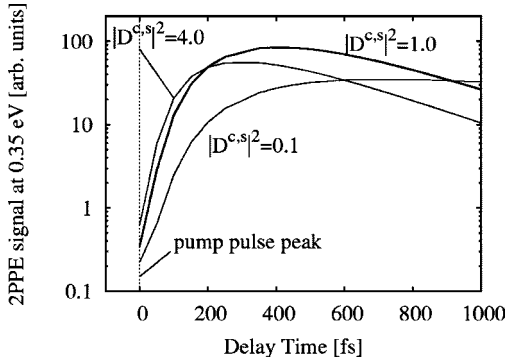

FIG. 10. 2PPE signal at 0.35 eV (originated from surface band) for resonant excitation into the surface state [situation (ii)] over delay time for different coupling strengths: $|D^{c,s}|^2=1.0$, $|D^{c,s}|^2=0.1$, and $|D^{c,s}|^2=4.0$.

this may change if the probe excitation strength is increased or the density of states is increased in a more realistic band structure calculation. Furthermore, Coulomb interaction might change the relative weight of the different contributions since it reduces the quasi-one-dimensional density of states at normal emission from the surface.

However, the most dominant signature for the off-resonant excitation is, that in strong contrast to situation (i), the signal dynamics arising from the surface band peak cannot be related in a simple way to a interband coupling strength because the signal decay does not scale directly with the coupling strength (cf. $|D^{c,s}|^2=1.0$ and $|D^{c,s}|^2=4.0$ in Fig. 10). The nonsystematic behavior, observed in Fig. 10, can only be explained by the interplay between the scattering into and out of the surface band, as well as the relaxation inside the surface and the bulk band. Therefore, the dynamics is in general not determined by the coupling constant $|D^{c,s}|^2$ alone. For example, the surface signal, depicted in Fig. 10, shows for the intermediate ($|D^{c,s}|^2=1.0$) and the strong ($|D^{c,s}|^2=4.0$) coupling a very similar rise (0–100 fs) and decay (600–1000 fs). In contrast, in the case of weak coupling ($|D^{c,s}|^2=0.1$), the signal rise is drastically slower (up to 1 ps) compared to all other time scales observed. This indicates, that the relaxation dynamics within the bulk conduction band transferring electrons to the conduction band minimum (which is slower than the surface-bulk coupling) dominates the depopulation of the surface band in the case of the intermediate and strong coupling. Furthermore, the surface-bulk scattering for the weak coupling is apparently even slower than the intraband scattering in the bulk conduction band. All in all, Fig. 10 demonstrates that the scattering times can not be extracted as easily as in the case of an initial population of the surface band [situation (i)], because the signal from the surface states are strongly affected by the relaxation inside the bulk conduction band, which—vice versa—is not influenced by the bulk-surface coupling.

VI. CONCLUSION

In the present work, we have developed a model for the ultrafast surface dynamics of electrons in semiconductors, taking into account two-dimensional surface states and three-dimensional semiconductor states as well as vacuum states. The coupling to a phonon bath and a classical electric field has been taken into account. The equations of motion for electronic transitions and occupations have been derived within Markovian and second-order Born approximations. Using a model four band system, including one surface band, the electron dynamics after optical excitation and corresponding TR-2PPE spectra have been investigated. It has been shown that if the surface state is resonantly excited, the resulting time resolved two pulse photoemission spectra can directly reveal the information of the underlying occupation dynamics and provide a measure for the coupling strength.

Our results should be viewed as a qualitative approach which can be improved later on by calculating the matrix elements in Eqs. (B1) and (B2) with *ab initio* wave functions and further interaction mechanisms such as electron-electron interaction.

ACKNOWLEDGMENTS

We thank the Deutsche Forschungsgemeinschaft for financial support through the Schwerpunktprogramm SP 1093. We thank L. Töben, F. Willig, P. Hahn, W. G. Schmidt, F. Bechstedt, P. Kratzer, and M. Scheffler for useful discussions.

APPENDIX A: CORRELATION EXPANSION AND EQUATIONS OF MOTION

The correlation expansion[33] of the operators leads to

$$\langle a_{\mathbf{k}}^{\alpha\dagger}a_{\mathbf{k}'}^{\alpha'}\rangle=\langle a_{\mathbf{k}}^{\alpha\dagger}a_{\mathbf{k}'}^{\alpha'}\rangle^c,\quad \langle b_{\mathbf{q}}^{\kappa\dagger}\rangle=\langle b_{\mathbf{q}}^{\kappa\dagger}\rangle^c,$$

$$\langle b_{\mathbf{q}}^{\kappa(\dagger)}b_{\mathbf{q}'}^{\kappa'(\dagger)}\rangle=\langle b_{\mathbf{q}}^{\kappa(\dagger)}b_{\mathbf{q}'}^{\kappa'(\dagger)}\rangle^c+\langle b_{\mathbf{q}}^{\kappa(\dagger)}\rangle^c\langle b_{\mathbf{q}'}^{\kappa'(\dagger)}\rangle^c,$$

$$\langle a_{\mathbf{k}}^{\alpha\dagger}a_{\mathbf{k}'}^{\alpha'}b_{\mathbf{q}}^{\kappa(\dagger)}\rangle=\langle a_{\mathbf{k}}^{\alpha\dagger}a_{\mathbf{k}'}^{\alpha'}b_{\mathbf{q}}^{\kappa(\dagger)}\rangle^c+\langle a_{\mathbf{k}}^{\alpha\dagger}a_{\mathbf{k}'}^{\alpha'}\rangle^c\langle b_{\mathbf{q}}^{\kappa(\dagger)}\rangle^c,$$

$$\begin{aligned}\langle a_{\mathbf{k}}^{\alpha\dagger}a_{\mathbf{k}'}^{\alpha'}b_{\mathbf{q}}^{\kappa(\dagger)}b_{\mathbf{q}'}^{\kappa'(\dagger)}\rangle&=\langle a_{\mathbf{k}}^{\alpha\dagger}a_{\mathbf{k}'}^{\alpha'}b_{\mathbf{q}}^{\kappa(\dagger)\kappa'(\dagger)}\rangle^c+\langle a_{\mathbf{k}}^{\alpha\dagger}a_{\mathbf{k}'}^{\alpha'}\rangle^c\langle b_{\mathbf{q}}^{\kappa(\dagger)}b_{\mathbf{q}'}^{\kappa'(\dagger)}\rangle^c\\&+\langle a_{\mathbf{k}}^{\alpha\dagger}a_{\mathbf{k}'}^{\alpha'}b_{\mathbf{q}'}^{\kappa'(\dagger)}\rangle^c\langle b_{\mathbf{q}}^{\kappa(\dagger)}\rangle^c+\langle a_{\mathbf{k}}^{\alpha\dagger}a_{\mathbf{k}'}^{\alpha'}b_{\mathbf{q}}^{\kappa(\dagger)}\rangle^c\langle b_{\mathbf{q}'}^{\kappa'(\dagger)}\rangle^c\\&+\langle a_{\mathbf{k}}^{\alpha\dagger}a_{\mathbf{k}'}^{\alpha'}\rangle^c\langle b_{\mathbf{q}}^{\kappa(\dagger)}\rangle^c\langle b_{\mathbf{q}'}^{\kappa'(\dagger)}\rangle^c,\end{aligned}$$

$$\begin{aligned}\langle a_{\mathbf{k}}^{\alpha\dagger}a_{\mathbf{l}}^{\beta\dagger}a_{\mathbf{k}'}^{\alpha'}a_{\mathbf{l}'}^{\beta'}\rangle&=\langle a_{\mathbf{k}}^{\alpha\dagger}a_{\mathbf{l}}^{\beta\dagger}a_{\mathbf{k}'}^{\alpha'}a_{\mathbf{l}'}^{\beta'}\rangle^c+\langle a_{\mathbf{k}}^{\alpha\dagger}a_{\mathbf{l}'}^{\beta'}\rangle^c\langle a_{\mathbf{l}}^{\beta\dagger}a_{\mathbf{k}'}^{\alpha'}\rangle^c\\&-\langle a_{\mathbf{k}}^{\alpha\dagger}a_{\mathbf{k}'}^{\alpha'}\rangle^c\langle a_{\mathbf{l}}^{\beta\dagger}a_{\mathbf{l}'}^{\beta'}\rangle^c.\end{aligned}\tag{A1}$$

The equation of motion of the electronic occupations and transitions, assuming that the energies include the polaron shift, read

$$\frac{d}{dt}\langle a_{\mathbf{k}}^{\alpha\dagger}a_{\mathbf{l}}^{\beta}\rangle=i(\epsilon_{\mathbf{k}}^{\alpha}-\epsilon_{\mathbf{l}}^{\beta})\langle a_{\mathbf{k}}^{\alpha\dagger}a_{\mathbf{l}}^{\beta}\rangle-\sum_{\alpha',\mathbf{k}'}\Omega_{\mathbf{k}',\mathbf{k}}^{\alpha'\alpha}\langle a_{\mathbf{k}'}^{\alpha'\dagger}a_{\mathbf{k}}^{\alpha}\rangle+\sum_{\beta',\mathbf{l}'}\Omega_{\mathbf{l}\mathbf{l}'}^{\beta,\beta'}\langle a_{\mathbf{l}}^{\beta\dagger}a_{\mathbf{l}'}^{\beta'}\rangle-\frac{\pi}{\hbar^2}\sum_{\substack{\beta',\gamma,\gamma',\kappa,\kappa',\pm\\\mathbf{l}',\mathbf{m},\mathbf{m}',\mathbf{q},\mathbf{q}'}}D_{\mathbf{l},\mathbf{l}',\mathbf{q}}^{\beta,\beta',\kappa}\overline{D}_{\mathbf{m},\mathbf{m}'\mathbf{q}'}^{\gamma,\gamma',\kappa'}\delta(\epsilon_{\mathbf{m}}^{\gamma}-\epsilon_{\mathbf{m}'}^{\gamma'}\mp\omega_{\pm\mathbf{q}'}^{\kappa'})$$

$$\times\left[\left(n_{\mathbf{q}'}^{\kappa'}+\frac{1}{2}\pm\frac{1}{2}\right)\langle a_{\mathbf{k}}^{\alpha\dagger}a_{\mathbf{m}}^{\gamma}\rangle(\delta_{\mathbf{m}',\mathbf{l}'}^{\gamma'\beta'}-\langle a_{\mathbf{m}'}^{\gamma',\dagger}a_{\mathbf{l}'}^{\beta'}\rangle)-\left(n_{\mathbf{q}'}^{\kappa'}+\frac{1}{2}\mp\frac{1}{2}\right)(\delta_{\mathbf{k},\mathbf{m}}^{\alpha,\gamma}-\langle a_{\mathbf{k}}^{\alpha\dagger}a_{\mathbf{m}}^{\gamma}\rangle)\langle a_{\mathbf{m}'}^{\gamma',\dagger}a_{\mathbf{l}'}^{\beta'}\rangle\right]$$

$$-\frac{\pi}{\hbar^2}\sum_{\substack{\alpha',\gamma,\gamma',\kappa\kappa',\pm\\ \mathbf{k}',\mathbf{m},\mathbf{m}',\mathbf{q},\mathbf{q}'}}\overline{D}^{\alpha,\alpha',\kappa}_{\mathbf{k},\mathbf{k}',\mathbf{q}}D^{\gamma,\gamma'\kappa'}_{\mathbf{m},\mathbf{m}'\mathbf{q}'}\delta(\epsilon^{\gamma'}_{\mathbf{m}'}-\epsilon^{\gamma}_{\mathbf{m}}\pm\omega^{\kappa'}_{\pm\mathbf{q}'})\Bigg[\left(n^{\kappa'}_{\mathbf{q}'}+\frac{1}{2}\pm\frac{1}{2}\right)\langle a^{\gamma\dagger}_{\mathbf{m}}a^{\beta}_{\mathbf{l}}\rangle(\delta^{\beta'\gamma'}_{\mathbf{l}',\mathbf{m}'}-\langle a^{\beta'\dagger}_{\mathbf{l}'}a^{\gamma'}_{m'}\rangle)$$
$$-\left(n^{\kappa'}_{\mathbf{q}'}+\frac{1}{2}\mp\frac{1}{2}\right)(\delta^{\gamma,\beta}_{\mathbf{m},\mathbf{l}}-\langle a^{\gamma\dagger}_{\mathbf{m}}a^{\beta}_{\mathbf{l}}\rangle)\langle a^{\beta'\dagger}_{\mathbf{l}'}a^{\gamma'}_{m'}\rangle\Bigg]. \tag{A2}$$

APPENDIX B: MATRIX ELEMENTS

The dipole moments

$$\mathbf{d}^{\alpha',\alpha}_{\mathbf{k}',\mathbf{k}}=S^{-1}_{\mathrm{EC}}\int d^3\mathbf{r}\,\overline{\psi}^{\alpha'}_{\mathbf{k}'}(\mathbf{r})(e\mathbf{r})\psi^{\alpha}_{\mathbf{k}}(\mathbf{r})$$

of the model wave equations, Sec. IV, give

$$\mathbf{d}^{[v,k^{(v)}_z],[c,k^{(c)}_z]}_{\mathbf{k}^{(v)},\mathbf{k}^{(c)}}=\delta_{\mathbf{k}^{(v)},\mathbf{k}^{(c)}}\delta_{k^{(v)}_z,k^{(c)}_z}\mathbf{d}^{v,c},$$

$$\mathbf{d}^{[c,k^{(c)}_z],s}_{\mathbf{k}^{(c)},\mathbf{k}^{(s)}}=\delta_{\mathbf{k}^{(c)},\mathbf{k}^{(s)}}(L_z)^{-1/2}\frac{i\Lambda^{1/2}_s}{-k^{(c)}_z+i\Lambda_s/2}\mathbf{d}^{c,s},$$

$$\mathbf{d}^{[c,k^{(c)}_z],[f,k^{(f)}_z]}_{\mathbf{k}^{(c)},\mathbf{k}^{(f)}}=\delta_{\mathbf{k}^{(c)},\mathbf{k}^{(f)}}(L_z)^{-1/2}\frac{iC_fT}{k^{(f,\mathrm{i})}_z-k^{(c)}_z+i\Lambda_f/2}\mathbf{d}^{c,f},$$

$$\mathbf{d}^{s,[f,k^{(f)}_z]}_{\mathbf{k}^{(s)},\mathbf{k}^{(f)}}=\delta_{\mathbf{k}^{(s)},\mathbf{k}^{(f)}}\frac{i\Lambda^{1/2}_sC_fT}{k^{(\mathrm{fi})}_z+i(\Lambda_s+\Lambda_f)/2}\mathbf{d}^{s,f}. \tag{B1}$$

The corresponding electron-phonon coupling elements

$$D^{\alpha,\alpha',\mathrm{LO}}_{\mathbf{k},\mathbf{k}',\mathbf{q}^{3\mathrm{d}}}=\sqrt{\frac{e^2\hbar\omega_{\mathrm{LO}}}{2SL\varepsilon_0\epsilon_{\mathrm{Phon}}}}\delta(\mathbf{k}'-\mathbf{k}+\mathbf{q}^{3d}_{\parallel})\Delta^{\alpha,\alpha'}_{q^{3\mathrm{d}}_z}$$

for the four band model system read

$$\Delta^{(c,k_z),(c,k'_z)}_{q_z}=\delta(k'_z-k_z+q_z),$$

$$\Delta^{(v,k_z),(v,k'_z)}_{q_z}=\delta(k'_z-k_z+q_z),$$

$$\Delta^{s,s}_{q_z}=\frac{i\Lambda_s}{q_z+i\Lambda_s},\quad \Delta^{(c,k_z),s}_{q_z}=\frac{iL^{-1/2}_z\Lambda^{1/2}_s}{q_z-k_z+i\Lambda_s/2}D_{c,s}. \tag{B2}$$

The remaining term

$$D^{c,s}=V^{-1}_{\mathrm{EC}}\int d^3\mathbf{r}\overline{u^c}(\mathbf{r})u^s(\mathbf{r})$$

is used as a fitting parameter which controls the strength of the coupling between the bulk conduction band and the surface band.

APPENDIX C: RWA EQUATIONS

The contribution from the free motion and the electric field

$$\left.\frac{d}{dt}\langle a^{\alpha'\dagger}_{\mathbf{k}'}a^{\alpha}_{\mathbf{k}}\rangle\right|_{\mathrm{field}}$$

for the subsystem containing bulk conduction band (c), surface band (s), and vacuum electrons (f) is given in rotating wave approximation with respect to the laser frequency ω_L. For simplicity the occupations and transitions are abbreviated as

$$P^{\alpha',\alpha}_{\mathbf{k}',\mathbf{k}}=\langle a^{\alpha'\dagger}_{\mathbf{k}'}a^{\alpha}_{\mathbf{k}}\rangle.$$

The laser field is written as

$$\mathbf{E}(t)=\mathrm{Re}[\mathbf{E}^e(t)\exp(i\omega_Lt)],$$

where $\mathbf{E}^e$ is a slowly varying envelope, including the phase shift. For abbreviation, the complex conjugate field amplitudes

$$\mathbf{E}^-=\frac{\overline{\mathbf{E}}^e(t)}{2},\quad \mathbf{E}^+=\frac{\mathbf{E}^e(t)}{2}$$

are introduced. For the subsystem containing bulk conduction band (c), surface band (s), and vacuum states (f), the corresponding equations of motion read

$$\dot{P}^{(c,k'_z),(c,k_z)}_{\mathbf{k},\mathbf{k}}=i(\epsilon^{c,k'_z}_{\mathbf{k}}-\epsilon^{c,k_z}_{\mathbf{k}})P^{(c,k'_z),(c,k_z)}_{\mathbf{k},\mathbf{k}}+\frac{i}{\hbar}\Bigg[\sum_{k''_z}\mathbf{E}^-\cdot\mathbf{d}^{(c,k_z),(f,k''_z)}_{\mathbf{k}\mathbf{k}}\overline{P}^{(f,k''_z),(c,k'_z)}_{\mathbf{k},\mathbf{k}}-\sum_{k''_z}\mathbf{E}^-\cdot\overline{\mathbf{d}}^{(c,k'_z)(f,k''_z)}_{\mathbf{k},\mathbf{k}}P^{(f,k''_z),(c,k_z)}_{\mathbf{k},\mathbf{k}}\Bigg],$$

$$\dot{P}^{s,(c,k_z)}_{\mathbf{k},\mathbf{k}}=i(\epsilon^{s}_{\mathbf{k}}-\epsilon^{c,k_z}_{\mathbf{k}})P^{s,(c,k_z)}_{\mathbf{k},\mathbf{k}}+\frac{i}{\hbar}\Bigg[\sum_{k''_z}\mathbf{E}^-\cdot\mathbf{d}^{(c,k_z),(f,k''_z)}_{\mathbf{k},\mathbf{k}}\overline{P}^{(f,k''_z),s}_{\mathbf{k},\mathbf{k}}-\sum_{k''_z}\mathbf{E}^-\cdot\overline{\mathbf{d}}^{s,(f,k''_z)}_{\mathbf{k},\mathbf{k}}P^{(f,k''_z),(c,k_z)}_{\mathbf{k},\mathbf{k}}\Bigg],$$

$$\dot{P}^{s,s}_{\mathbf{k},\mathbf{k}}=i(\epsilon^{s}_{\mathbf{k}}-\epsilon^{s}_{\mathbf{k}})P^{s,s}_{\mathbf{k},\mathbf{k}}+\frac{i}{\hbar}\Bigg[\sum_{k''_z}\mathbf{E}^-\cdot\mathbf{d}^{s,(f,k''_z)}_{\mathbf{k},\mathbf{k}}\overline{P}^{(f,k''_z),s}_{\mathbf{k},\mathbf{k}}-\sum_{k''_z}\mathbf{E}^-\cdot\overline{\mathbf{d}}^{s,(f,k''_z)}_{\mathbf{k},\mathbf{k}}P^{(f,k''_z),s}_{\mathbf{k},\mathbf{k}}\Bigg],$$

$$\dot{P}^{(f,k_z'),(c,k_z)}_{\mathbf{k},\mathbf{k}} = i(\epsilon^{f,k_z'}_{\mathbf{k}} - \epsilon^{c,k_z}_{\mathbf{k}} - \omega_L)P^{(f,k_z'),(c,k_z)}_{\mathbf{k},\mathbf{k}} + \frac{i}{\hbar}\left[\sum_{k_z''} \mathbf{E}^+ \cdot \mathbf{d}^{(c,k_z),(f,k_z'')}_{\mathbf{k},\mathbf{k}} P^{(f,k_z'),(f,k_z'')}_{\mathbf{k},\mathbf{k}} - \sum \mathbf{E}^+_{\cdot k_z''} \mathbf{d}^{(c,k_z''),(f,k_z')}_{\mathbf{k},\mathbf{k}} P^{(c,k_z''),(c,k_z)}_{\mathbf{k},\mathbf{k}}\right] - \frac{i}{\hbar}\mathbf{E}^+ \cdot \mathbf{d}^{s,(f,k_z')}_{\mathbf{k},\mathbf{k}} P^{s,(c,k_z)}_{\mathbf{k},\mathbf{k}},$$

$$\dot{P}^{(f,k_z),s}_{\mathbf{k},\mathbf{k}} = i(\epsilon^{f,k_z}_{\mathbf{k}} - \epsilon^{s}_{\mathbf{k}} - \omega_L)P^{(f,k_z),s}_{\mathbf{k},\mathbf{k}} - \frac{i}{\hbar}\sum_{k_z''} \mathbf{E}^+ \cdot \mathbf{d}^{(c,k_z''),(f,k_z)}_{\mathbf{k},\mathbf{k}} \overline{P}^{s,(c,k_z'')}_{\mathbf{k},\mathbf{k}} + \frac{i}{\hbar}\left[-\mathbf{E}^+ \cdot \mathbf{d}^{s,(f,k_z)}_{\mathbf{k},\mathbf{k}} P^{s,s}_{\mathbf{k},\mathbf{k}} + \sum_{k_z''} \mathbf{E}^+ \cdot \mathbf{d}^{s,(f,k_z'')}_{\mathbf{k},\mathbf{k}} P^{(f,k_z),(f,k_z'')}_{\mathbf{k},\mathbf{k}}\right],$$

$$\dot{P}^{(f,k_z'),(f,k_z)}_{\mathbf{k},\mathbf{k}} = i(\epsilon^{f,k_z'}_{\mathbf{k}} - \epsilon^{f,k_z}_{\mathbf{k}})P^{(f,k_z'),(f,k_z)}_{\mathbf{k},\mathbf{k}} + \frac{i}{\hbar}\left[\sum_{k_z''} \mathbf{E}^- \cdot \overline{\mathbf{d}}^{(c,k_z''),(f,k_z)}_{\mathbf{k},\mathbf{k}} P^{(f,k_z'),(c,k_z'')}_{\mathbf{k},\mathbf{k}} - \sum_{k_z''} \mathbf{E}^- \cdot \mathbf{d}^{(c,k_z''),(f,k_z')}_{\mathbf{k},\mathbf{k}} \overline{P}^{(f,k_z),(c,k_z'')}_{\mathbf{k},\mathbf{k}}\right] + \frac{i}{\hbar}[\mathbf{E}^- \cdot \overline{\mathbf{d}}^{s,(f,k_z)}_{\mathbf{k},\mathbf{k}} P^{(f,k_z'),s}_{\mathbf{k},\mathbf{k}} - \mathbf{E}^- \cdot \mathbf{d}^{s,(f,k_z')}_{\mathbf{k},\mathbf{k}} \overline{P}^{(f,k_z),s}_{\mathbf{k},\mathbf{k}}].$$

.

APPENDIX D: PHONON INTERACTION

As an example, the diagonal scattering rate from the surface band into the bulk conduction band is given. It reads

$$(\Gamma^s_{\mathbf{k}})^{\to c} = \frac{\pi}{\hbar^2}\sum_{q_z,k_z,\pm} \frac{e^2 m^c_{\mathrm{eff}}\omega_{\mathrm{LO}}}{4\pi L \epsilon_0 \varepsilon_{\mathrm{phon}}} |\Delta^{(c,k_z),s}_{q_z}|^2 \Theta(K^2_{\mp}) \times \{[(k-K_{\mp})^2 + q_z^2][(k+K_{\mp})+q_z^2]\}^{-1/2}, \quad \text{(D1)}$$

where

$$K^{\mp} = \left\{\frac{2m^s_{\mathrm{eff}}}{\hbar^2}\left[E^c_0 - E^s_0 + \frac{\hbar^2}{2m^c_{\mathrm{eff}}}(k_z^2 + k^2) \mp \hbar\omega_{\mathrm{LO}}\right]\right\}^{-1/2}$$

and Θ is the step function.

*Email address: zeiser@itp.physik.tu-berlin

[1] T. Hertel, E. Knoesel, M. Wolf, and G. Ertl, Phys. Rev. Lett. **76**, 535 (1996).
[2] E. Knoesel, A. Hotzel, and M. Wolf, Phys. Rev. B **57**, 12812 (1998).
[3] U. Höfer, I. L. Shumay, C. Reuß, U. Thomann, W. Wallauer, and T. Fauster, Science **277**, 1480 (1997).
[4] C. B. Harris, N. H. Ge, R. L. Lingle, Jr., J. D. McNeill, and C. M. Wong, Annu. Rev. Phys. Chem. **48**, 711 (1997).
[5] H. Petek and S. Ogawa, Prog. Surf. Sci. **59**, 239 (1998).
[6] C. Gahl, K. Ishioka, Q. Zhong, A. Hotzel, and M. Wolf, Faraday Discuss. **117**, 191 (2001).
[7] Q. Zhong, C. Gahl, and M. Wolf, Surf. Sci. **496**, 21 (2002).
[8] S. Jeong and J. Bokor, Phys. Rev. B **59**, 4943 (1999).
[9] J. K. Goldmann and J. A. Prybyla, Phys. Rev. Lett. **72**, 1364 (1994).
[10] C. Schmuttenmaer, C. C. Miller, J. W. Herman, J. Cao, D. A. Mantell, Y. Gao, and R. J. D. Miller, Chem. Phys. **205**, 91 (1996).
[11] W. S. Fann, R. Storz, H. W. K. Tom, and J. Bokor, Phys. Rev. Lett. **68**, 2834 (1992).
[12] C. A. Schmuttenmaer, M. Aeschlimann, H. E. Elsayed-Ali, R. J. D. Miller, D. A. Mantell, J. Cao, and Y. Gao, Phys. Rev. B **50**, 8957 (1994).
[13] L. Töben, Ph.D. thesis, TU Berlin, Shaker, Aachen, 2002.
[14] L. Töben, L. Gundlach, T. Hannappel, R. Ernstorfer, R. Eichberger, and F. Willig, Appl. Phys. A: Mater. Sci. Process. **78**, 239 (2004).
[15] M. Weinelt, M. Kutschera, T. Fauster, and M. Rohlfing, Phys. Rev. Lett. **92**, 126801 (2004).
[16] R. Haight, Surf. Sci. Rep. **21**, 275 (1995).
[17] A. Rettenberger and R. Haight, Phys. Rev. Lett. **76**, 1912 (1996).
[18] T. Klamroth, P. Saalfrank, and U. Höfer, Phys. Rev. B **64**, 035420 (2001).
[19] S. Jorgenson, M. Ratner, and K. Mikkelsen, J. Chem. Phys. **115**, 4314 (2001).
[20] H. Ueba, Surf. Sci. **334**, L719 (1995).
[21] S. Ramakrishna, F. Willig, and A. Knorr, Appl. Phys. A: Mater. Sci. Process. **78**, 247 (2004).
[22] S. Ramakrishna, F. Willig, and A. Knorr, Surf. Sci. **558**, 159 (2004).
[23] A. Zeiser, N. Bücking, J. Götte, J. Förstner, P. Hahn, W. G. Schmidt, and A. Knorr, Phys. Status Solidi B **241**, R60 (2004).
[24] T. Kuhn, in *Theory of Transport Properties of Semiconductor Nanostructures*, edited by E. Schöll (Chapman and Hall, London, 1998), p. 173.
[25] I. Waldmüller, J. Förstner, S.-C. Lee, A. Knorr, M. Woerner, K. Reimann, R. A. Kaindl, T. Elsaesser, R. Hey, and K. H. Ploog, Phys. Rev. B **69**, 205307 (2004).
[26] P. Lambropoulos and P. Zoller, Phys. Rev. A **24**, 379 (1981).
[27] L. Töben, L. Gundlach, R. Ernstorfer, R. Eichberger, T. Hannappel, F. Willig, A. Zeiser, J. Förstner, A. Knorr, P. H. Hahn *et al.*, Phys. Rev. Lett. **94**, 067601 (2005).
[28] F. Bechstedt, *Principles of Surface Science* (Springer, Berlin, 2003).
[29] W. Schmidt and F. Bechstedt, Surf. Sci. **409**, 474 (1998).

[30] W. G. Schmidt, N. Esser, A. M. Frisch, P. Vogt, J. Bernholc, F. Bechstedt, M. Zorn, T. Hannappel, S. Visbeck, F. Willig *et al.*, Phys. Rev. B **61**, R16335 (2000).

[31] H. Haug and S. W. Koch, *Quantum Theory of the Optical and Electronic Properties of Semiconductors*, 3rd ed. (World Scientific, Singapore, 1990).

[32] M. Lindberg and S. W. Koch, Phys. Rev. B **38**, 3342 (1988).

[33] J. Fricke, Ann. Phys. **252**, 479 (1996).

[34] M. Reichelt, T. Meier, S. W. Koch, and M. Rohlfing, Phys. Rev. B **68**, 045330 (2003); C. Voelkmann, M. Reichelt, T. Meier, S. W. Koch, and U. Höfer, Phys. Rev. Lett. **92**, 127405 (2004).

[35] M. C. Desjonquères and D. Spanjaard, *Concepts in Surface Physics*, 2nd ed. (Springer, Berlin, 1996).

[36] P. Hahn, W. Schmidt, and F. Bechstedt, Institut für Festkörpertheorie und -optik, Universität Jena.

[37] G. D. Mahan, in *Photoemission and Absorption Spectroscopy of Solids and Interfaces with Synchrotron Radiation*, edited by M. Campagna and R. Rosei (North-Holland, Amsterdam, 1990), pp. 25–40.

[38] S. Lorenz, C. Solterbeck, W. Schattke, J. Burmeister, and W. Hackbusch, Phys. Rev. B **55**, R13432 (1997).

[39] L. Allen and J. Eberly, *Optical Resonance and Two-Level Atoms* (Dover, New York, 1975).

[40] U. Hohenester, P. Supancic, P. Kocevar, X. Q. Zhou, W. Kütt, and H. Kurz, Phys. Rev. B **47**, 13233 (1993).

[41] A. M. Frisch, P. Vogt, S. Visbeck, T. Hannappel, F. Willig, W. Braun, W. Richter, J. Bernholc, W. G. Schmidt, and N. Esser, Appl. Surf. Sci. **166**, 224 (2000).

[42] P. Y. Yu and M. Cardona, *Fundamentals of Semiconductors*, 2nd ed. (Springer, Berlin, 1996).